Journal of Nuclear Materials 376 (2008) 216–221

Contents lists available at ScienceDirect

Journal of Nuclear Materials

journal homepage: www.elsevier.com/locate/jnucmat

First temperature stage evolution of irradiation-induced defects in tungsten studied by positron annihilation spectroscopy

A. Debelle *, M.F. Barthe, T. Sauvage

CNRS-CEMHTI, 3A Rue de la Férollerie, 45071 ORLEANS cedex 2, France

ARTICLE INFO

Article history:
Received 23 November 2007
Accepted 3 March 2008

PACS:
61.80.−x
61.72.Ji
78.70.Bj
61.82.Bg

ABSTRACT

The behaviour of vacancy like implantation-induced defects created in the track region of 800 keV ^{3}He ions in polycrystalline tungsten was studied by Doppler broadening spectroscopy as a function of annealing temperature. A slow positron beam, coupled with a Doppler broadening spectrometer, was used to measure the low- and high-momentum annihilation fractions, *S* and *W*, respectively, as a function of positron energy in tungsten samples implanted at different fluences from 10^{14} to 5×10^{16} cm^{-2}. The behaviour of the *S*(*E*), *W*(*E*) and *S*(*W*) plots with the annealing temperature clearly indicates that the irradiation-induced vacancy like defects begin to evolve between 523 and 573 K, whatever the implantation fluence. This first temperature stage evolution corresponds to the migration of the monovacancies created during implantation to form larger vacancy like defects of which depth profile is different from the initial radiation-induced defects one.

1. Introduction

In the future International Thermonuclear Experimental Reactor (ITER), tungsten, due to its intrinsic physical properties, such as high fusion temperature ($T_f \sim 3693$ K), low sputtering yield with light elements and good thermo-mechanical behaviour, is a potential candidate material to cover some parts of the divertor in controlled fusion experiments. The divertor, as a plasma-facing-component, will be subjected to intense irradiations at possible high temperature (up to 1273 K). The development and qualification of materials capable of withstanding such extreme conditions is a critical step towards the realization of the future nuclear systems. In the specific case of fusion reactor, high 14 MeV neutrons flux will cause the continuous production of both H and He by (n,p) and (n,α) nuclear reactions, and of irradiation-induced defects by recoils. It is well-known that the combined presence of gas and defects often leads to microstructural and morphological modifications in the materials, such as bubbles formation and blistering, which in turn will cause physical and mechanical changes [1] [and references therein]. Therefore, determining if the tungsten is effectively capable to resist to these severe conditions requires a thorough understanding of the gas (He and H) interaction with the radiation-induced defects. Obviously, it first requires to accurately characterise these defects. To address this issue, the CEMHTI (former CERI) uses its accelerators to produce and characterize the defects, the characterisation being especially achieved with positron annihilation spectroscopy (PAS) techniques, which have proven to be successful in the detection and identification of point defects on an atomic scale.

The study by PAS of defects created in tungsten, either by ion implantation or irradiation, has already been the scope of several research works [2–5]; besides, the defects evolution upon subsequent thermal treatment has also been investigated [2,4,6,7]. From the obtained results, the following four steps scheme can be drawn: (i) stage zero (0), from room temperature (RT) to ∼573 K: a possible dissociation of small vacancy–impurity (V–Im) complexes can arise, leading to an increase of the concentration of small vacancies, principally monovacancies; (ii) stage one (I), from ∼573 K to ∼773 K: monovacancies migrate through the crystal lattice and either agglomerate with other vacancy like defects to form larger defects or annihilate at defects sinks such as grain boundaries; (iii) stage two (II), from ∼773 K to ∼1723 K: this stage is equivalent to stage one but for larger vacancy like clusters, which can migrate and annihilate at defects sinks or agglomerate to form small cavities; (iv) stage three (III), from ∼1723 K to ∼2773 K (the usual ∼0.7 T_f reference for complete recovery): anneal out of most of the vacancy like defects (large clusters and cavities). Hence, three important stages are clearly put forward: a stage of small vacancy-type defects migration at low temperature (relatively to the tungsten fusion temperature), a stage of stability of medium then large defects at intermediate temperature, and a last stage of defects recovery at high temperature. What appears less clear are the temperature boundaries of these stages, especially those of step one, which concerns the monovacancy migration. Indeed, despite that the energy [8–11] and temperature [6,7,12] migration of

* Corresponding author. Present address: Université Paris Sud 11, CSNSM, Bât 108, 91405 ORSAY cedex, France. Tel.: +33 1 69 15 39 95; fax: +33 1 69 15 52 68.
E-mail address: debelle@csnsm.in2p3.fr (A. Debelle).

0022-3115/$ - see front matter © 2008 Elsevier B.V. All rights reserved.
doi:10.1016/j.jnucmat.2008.03.002

the monovacancy in tungsten have been the scope of many studies, there is not actually an agreement on these values; for example, the monovacancy temperature migration is found to vary from 553 K to 873 K. This value must be specified since it is a fundamental and basic data necessary for a complete understanding of the vacancy like defects creation and evolution in temperature. Consequently, the present paper deals with the determination of the monovacancy migration temperature in tungsten; the resultant defects evolution is also examined.

2. Experimental details

2.1. Sample preparation

Four ~150 μm thick polycrystalline one side polished 99.95% pure tungsten samples (containing impurities such as Mo, Fe, C...), cut out of commercial laminated foils, were used for this study. Prior to implantation with helium ions (details of the implantations conditions will be given hereafter), they were thermally annealed (thermal treatment 2, TT2) during 6 h at 1538 K under vacuum in order to eliminate a large part of manufacturing/polishing defects, as will be shown further. Then, after implantation, samples were submitted to thermal treatments of 1 h under vacuum (base pressure of $\sim 10^{-8}$ mbar) at five different temperatures, 423 K, 523 K, 573 K, 623 K, and 673 K. This allowed determining the defects evolution with temperature. Note that for each fluence, the same sample was annealed at the different temperatures.

2.2. ^{3}He implantations

^{3}He implantations were performed with a 3.5 MV Van de Graaff accelerator at four fluences, 10^{14}, 10^{15}, 10^{16} and 5×10^{16} cm^{-2}, the corresponding mean flux being comprised between $\sim 6.5 \times 10^{10}$ and $\sim 2.5 \times 10^{12}$ cm^{-2} s^{-1}. The helium ions energy was fixed at 800 keV so that the projected range ($R_p \sim 1.2$ μm), calculated with the SRIM code [13], was beyond the positrons implantation profile (see below). To achieve homogeneous implantations, these latter were carried out by focusing the 8×8 mm^2 primary ion beam to a 1×1 mm^2 one and by sweeping it over the surface sample. Besides, during all experiments, the mean temperature of the sample holder was below 333 K.

2.3. Doppler broadening spectroscopy

The Doppler broadening measurements were performed by using a Doppler broadening spectrometer coupled to the positron accelerator (for a complete description of the accelerator, see [14]). This DBS measurement system is a standard gamma-spectroscopy system equipped with a high purity germanium detector that offers a high energy resolution (<1.3 keV at 511 keV) and a high efficiency (>25% at 1.33 MeV). The positron–electron pair momentum distribution has been measured at RT by recording the Doppler broadening of the 511 keV annihilation line characterised by the S and W integral parameters. S is defined by the ratio of the area calculated around the maximum of the peak in the momentum window ($0–|2.80| \times 10^{-3} m_0 c$), over the total number of annihilations. The m_0 and c parameters are respectively the rest mass of the electron and the speed of light. This S fraction corresponds to annihilations with low momentum electrons, thus more predominantly with valence electrons. W is defined by the ratio of the area calculated at the wings of the peak in the momentum windows ($|10.61|–|26.35| \times 10^{-3} m_0 c$), over the total number of annihilations. This W fraction corresponds to annihilations with high momentum electrons, thus it is essentially related to positron annihilations with core electrons. By varying the incident positrons energy, the depth dependence of S and W can be obtained. In the present case, $S(E)$ and $W(E)$ were recorded in the range 0.5–25 keV, the energy being changed in 0.5 keV steps; the total count rate was chosen so that a good statistic is ensured. This energy range corresponds to a mean positrons implantation depth in tungsten comprised between approximately 0.4 nm and 300 nm. Note that the full-width-at-half-maximum of the implanted positrons distribution increases with the energy, to reach ~380 nm at 25 keV. Thus, at this energy, positrons probe up to ~700 nm under the surface. Hence, positrons do not reach the 800 keV ^{3}He ions stopping zone, but probe the track region (TR), localized between the surface and the nuclear cascade region (CR), and corresponding to the zone where ions slow down mainly by electronic energy loss processes. A UO_2 disk, labelled B23, polished and thermally annealed at 1973 K during 24 h in humid Ar/H_2 atmosphere, was chosen as a sample reference. Indeed, in this disk, S and W values are close to the tungsten ones, and remain constant over a large energy range, 5–25 keV ($S_{B23} = 0.3713$ and $W_{B23} = 0.0791$). This reference sample allows checking the reproducibility of the measurements, especially the stability of the positron beam and of the DBS system. Therefore, all the S and W values given in this paper are normalised to the ones obtained in the UO_2 reference. For the reader convenience, the annihilation characteristics S and W of positrons obtained with the same system in a more used material, e.g. the silicon, are given in [15]. Note that each material exhibits specific S and W values, signature of the momentum electrons distribution in the lattice in the absence of vacancy defects. Thus, it is important to keep in mind that S increases and W decreases when positrons are trapped and annihilate in vacancy defects, and reversely.

Hereafter, a modified version of VEPFIT [16], which combines the calculation of the positrons implantation and their diffusion, is used to consistently fit the $S(E)$ and $W(E)$ curves. Note that the data below ~2.5 keV are discarded because in this energy range, the positrons migration is not due, in the present case, to a diffusion process.

3. Results and discussion

3.1. Radiation-induced defects

The study by DBS of the as-received and as-implanted tungsten samples has been published in a previous paper [17]. Four samples were submitted to a preparation thermal treatment (thermal treatment 1, TT1), 1773 K during 1 h under ArH_2 atmosphere in a tubular furnace, in order to anneal out most of the pre-existing defects; then, they were implanted with helium ions at fluences of 10^{15}, 10^{16}, 5×10^{16} and 10^{17} cm^{-2}. Vacancy-type defects have been detected by positrons after helium implantation and it was shown that their concentration increases with the implantation fluence. Nonetheless, a saturation phenomenon was observed at the highest fluence, 10^{17} cm^{-2}. The quantification of the radiation-induced damage, characterized by the displacements per atom (dpa) parameter and the median energy of the primary knock-on atoms, tends to suggest that the implantation-induced defects (in the TR) were most likely mono-vacancies (denoted V_1). The annihilation characteristics of positrons trapped in these defects have been evaluated at 0.417 ± 0.001 and 0.0576 ± 0.0005, respectively for S_{V_1} and W_{V_1} (see Fig. 1).

In the present study, a different preparation thermal treatment (thermal treatment 2, TT2) was achieved (see Section 2). Fig. 1 represents the low-momentum annihilation fraction (S) as a function of the high-momentum annihilation fraction (W) for the 20–25 keV positron energy range – where the contribution of annihilations at the material surface can be disregarded – measured in all

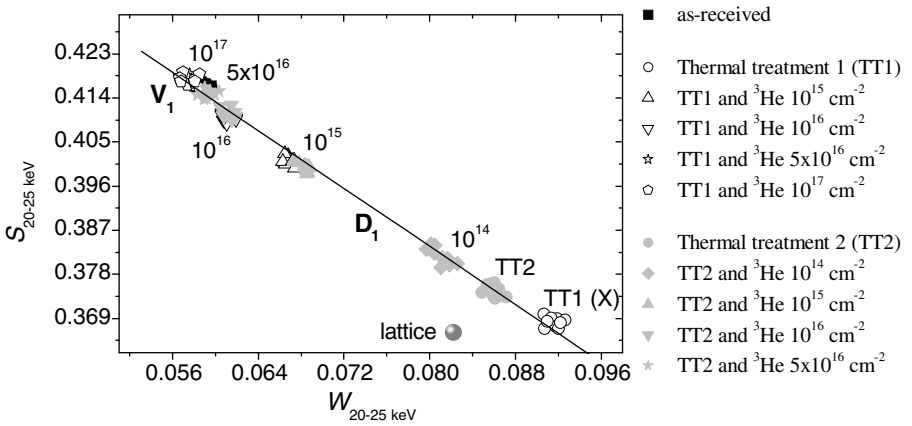

Fig. 1. Annihilation characteristics of 20–25 keV positrons in the track region of 800 keV ^{3}He ions implanted in polycrystalline tungsten at different fluences from 10^{14} cm^{-2} to 10^{17} cm^{-2}. Two sets of implantations were performed after different preparation thermal treatment: open symbols correspond to samples which have been prepared with TT1, and full symbols to samples prepared with TT2 (see text). V_1 designates the annihilation characteristics in the tungsten monovacancy (which are besides those found in as-received tungsten samples) and X the annihilation characteristics in the unidentified defects (see text for more details). Also plotted on this figure are the positron annihilation characteristics found in the tungsten lattice. D_1 is the line which passes through the annihilation characteristics in the lattice and in the monovacancy.

the different tungsten samples, i.e. prepared either with TT1 or TT2 and subsequently implanted. Also plotted are the positron annihilation characteristics in the as-received samples, which are equivalent to the characteristics in V_1 (see [17]). It can be seen that the positron annihilation characteristics in the tungsten samples prepared with TT2 are very close to the ones obtained in the samples prepared with TT1, and are all located on the line, D_1, which passes through the annihilation characteristics in the as-received tungsten samples and in the TT1 prepared tungsten samples. That means that a large part of the pre-existing vacancy-type defects were also eliminated after TT2 and that the two treatments lead to a very close state. The positron annihilation characteristics in the tungsten lattice, which were not yet determined for the previous study, are also plotted in Fig. 1. They have been extracted from the refinement with VEPFIT of the experimental data recorded in single-crystal tungsten samples annealed under vacuum at different temperatures ranging from 1473 K to 1873 K; in fact, the characteristics do not change from 1473 K. It is worth noticing that the characteristics corresponding to the annealed polycrystalline tungsten samples are not the lattice ones, even though a large part of the defects was annealed out and that a significant recrystallisation occurred [17]. Rather, they indicate the presence of positron traps of chemical nature, since the S values at the highest positron energy are almost equal to the ones in the lattice but the W values are larger. These unidentified defects (denoted hereafter as X) are possibly small clusters of impurities that have formed during the thermal treatment. This will be discussed in a forthcoming paper, but it is yet worth noticing that in the polycrystalline tungsten obtained after TT1, almost 100% of the positrons annihilate at these X defects, which signifies that the corresponding positron annihilation characteristics are the ones of the X defects.

To perform the study of the defects evolution as a function of annealing temperature, the following four fluences were chosen, 10^{14}, 10^{15}, 10^{16} and 5×10^{16} cm^{-2}, since a saturation phenomenon was observed at the highest fluence (10^{17} cm^{-2}) in the previous study. It can be seen in Fig. 1 that after implantation, the positron annihilation characteristics dramatically changed. That means that since, as will be shown latter, the X defects did not disappear during implantation, the positron affinity for the vacancy like radiation-induced defects is stronger than the one for the X defects.

At same implantation fluence, i.e. for 10^{15}, 10^{16} and 5×10^{16} cm^{-2}, the positron annihilation characteristics determined in the specimen prepared with one or the other of the thermal treatments are (nearly) equal. This clearly indicates that the same state is reached after implantation in both cases, and consequently, results obtained in the previous study can be applied to the present work. In particular, irradiation-induced defects created in the present study are also most likely monovacancies (V_1). Nonetheless, due to the purity of the material, the question of a possible formation of a complex with impurities (V_1–Im) can not be disregarded.

3.2. Defects evolution in temperature

Fig. 2 shows the evolution of the mean values of the S and W parameters in the 23–25 keV positron energy range for the four fluences as a function of the annealing temperature. The main result emerging from this figure is that two evolution stages can be identified: (i) from RT to 523 K, where no significant change in S and W is observed, and (ii) beyond to 523 K (until 673 K), where a notable evolution of these parameters occurs. It is worth mentioning that these two stages seem to correspond to stages zero (0) and one (I) presented in the introduction part. These two well marked domains are clearly visible for the two highest helium implantation fluences (for the two lowest fluences, it is likely that these two stages are present, but the variations of S and W are too weak to highlight a notable evolution; this will be discussed latter).

The case of the 10^{16} cm^{-2} fluence is now described in details. Fig. 3(a) and (b) shows the $S(E)$ and $W(E)$ curves of the 10^{16} cm^{-2} implanted tungsten sample for the six pre-cited temperatures. From RT to 523 K, the positron annihilation characteristics variations can be disregarded. Indeed, since positron energy of 6 keV, S and W reach, for the three temperatures (RT, 473 and 523 K), a same plateau value, traducing a homogeneous defects depth distribution, and indicating that no modification of the distribution nor of the nature of the defects occurred during the annealings. That means that none of the vacancy like defects present in the sample is mobile before 523 K, in agreement with the results found in the literature. Between 523 K and 573 K, an outright evolution of S and W is noticeable. Fig. 3(c) shows the $S(W)$ curves corresponding to annihilations of positrons of energy higher than 6 keV in the 10^{16} cm^{-2} implanted tungsten sample; only the curves for the three relevant temperatures, RT, 523 K and 673 K are displayed for clarity reasons. From 573 K, the $S(W)$ points deviate from the D_1 line, which traduces a change in the nature of the defects detected by the positrons. The higher slope of the new line, D_2, indicates the formation (and detection) of larger vacancy like defects, denoted hereafter as V_p, of which identification remains to

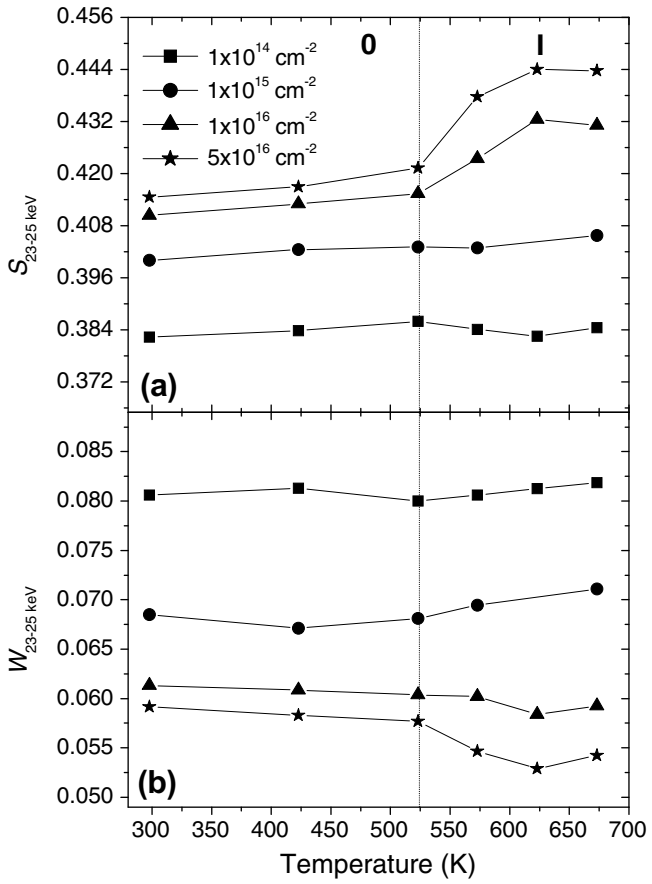

Fig. 2. Mean values of (a) the low-momentum (S) and (b) high-momentum (W) annihilation fractions at positron energy of 23–25 keV as a function of the annealing temperature (until 673 K) in the track region of 800 keV ^{3}He ions implanted in polycrystalline tungsten at four fluences from 10^{14} to 5×10^{16} cm^{-2}. '0' and 'I' represent the two annealing stages.

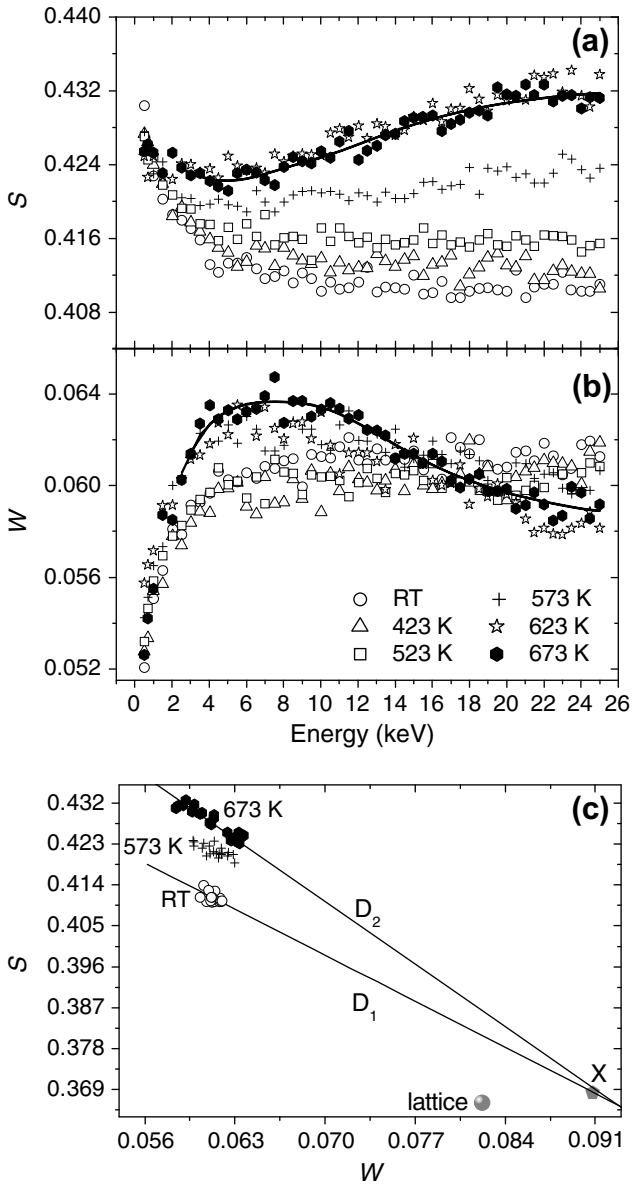

Fig. 3. (a) Low- (S) and (b) high- (W) momentum annihilation fractions as a function of the positron energy in the track region of 800 keV ^{3}He ions implanted at 10^{16} cm^{-2} in a polycrystalline tungsten sample annealed until 673 K; the black full lines correspond to the best fit with the VEPFIT program of the experimental data of the sample annealed at 673 K. The $S(W)$ plots corresponding to annihilations of positrons of energy higher than 6 keV (see text) for the three relevant temperatures (RT, 573 K and 673 K) are displayed on (c). Also plotted on this figure are the positron annihilation characteristics found in the tungsten lattice and in the unidentified X defects.

be performed. This is an important result since it clearly indicates that the first annealing stage in tungsten takes place between 523 K and 573 K. From the data available in the literature (see introduction part), this stage should correspond to the migration of V_1, which agglomerate to form V_p defects. Nonetheless, as previously mentioned, V_1 could have formed complexes with impurities during the implantation. In this case, the migration of the irradiation-induced defects observed at temperatures higher than 523 K could be in fact the result of two processes. First, the V_1–Im complexes start to migrate between 523 and 573 K; second, complexes dissociate at these temperatures, and the true migration temperature of the isolated V_1 is lower. An increase of the migration temperature of isolated vacancies due to a trapping by impurity atoms has already been reported, for example in the case of iron where monovacancies are trapped at carbon impurities [18]. Anyway, as far as plasma-facing materials (PFM) concern, it is not likely that highly pure material will be used in ITER and subsequent fusion reactors for evident cost reasons. Therefore, it is important to emphasize that monovacancies (isolated or associated with impurities) are mobile in commercial tungsten since 523–573 K, which is a relevant fundamental data for the wider study of interaction of light gases (helium, hydrogen) with vacancy-type defects in PFM.

The shape of the $S(E)$ and $W(E)$ curves also changed after annealing at temperatures higher than 523 K (see Fig. 3(a) and (b)). Curves can now be described as follow: S (respectively, W) decreases (respectively, increases) until positron energy of ~6 keV but then increases (respectively, decreases) until the maximum positron energy. This indicates that the defects distribution became inhomogeneous with depth, suggesting a concentration gradient. To confirm this assumption, a consistent fit, by using VEPFIT program, of both $S(E)$ and $W(E)$ curves corresponding to the 10^{16} cm^{-2} implanted sample and annealed at 673 K was performed; the corresponding curves, displayed on Fig. 3(a) and (b), show a fitting of good quality. The fitting parameters are listed in Table 1. Three homogeneous layers of different thickness, t, characterized by a very weak effective positron diffusion length, L_{eff}, were necessary to reproduce the experimental profiles (see Fig. 4); this modelling effectively allows accounting for a concentration gradient. Besides, this simulation also shows that none of the positron annihilation characteristics of the different layers is on the line

Table 1
List of the parameters describing the three layers required for the refinement with the VEPFIT program of the experimental profiles of the low-momentum annihilation fraction (S) and of the high-momentum annihilation fraction (W), as a function of positron energy in the track region of 800 keV ^{3}He ions implanted at 10^{16} cm^{-2} in a polycrystalline tungsten sample annealed at 673 K

Layer	S	W	t (nm)	L_{eff} (nm)
1	0.425	0.063	57	5.7
2	0.430	0.062	167	5.7
3	0.437	0.057	–	5.7

The layer thickness is referred as t, and L_{eff} is the effective positron diffusion length.

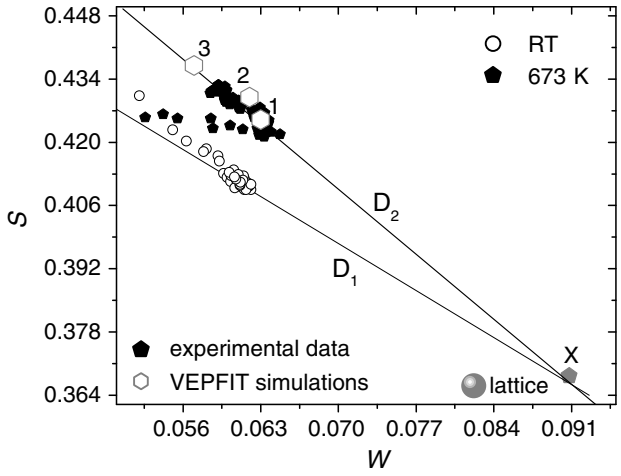

Fig. 4. Experimental low-momentum annihilation fraction (S) as a function of high-momentum annihilation fraction (W) in the track region of 800 keV ^{3}He ions implanted at 10^{16} cm^{-2} in a polycrystalline tungsten sample annealed at 673 K, and corresponding S and W values obtained by the fitting of the experimental data with the VEPFIT program. The numbers 1–3 represent the number of the different layers required to reproduce the experimental profiles (see Table 1). Also plotted on this figure are the positron annihilation characteristics found in the tungsten lattice and in the unidentified X defects.

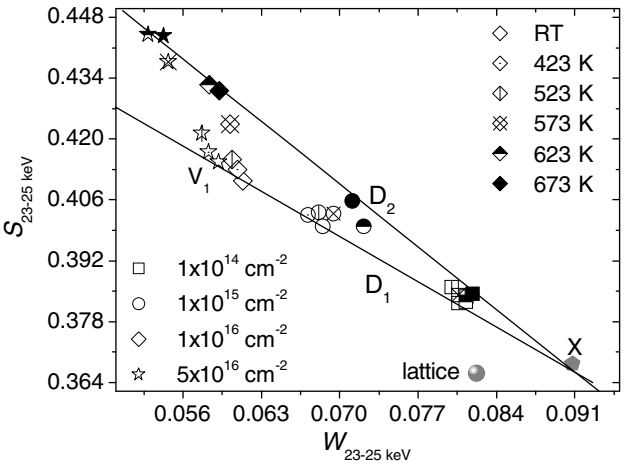

Fig. 5. Low-momentum annihilation fraction (S) as a function of high-momentum annihilation fraction (W) in the track region of 800 keV ^{3}He ions implanted at four fluences from 10^{14} to 5×10^{16} cm^{-2} in a polycrystalline tungsten sample annealed until a 673 K temperature. V_1 designates the annihilation characteristics in the tungsten monovacancy. Also plotted on this figure are the positron annihilation characteristics found in the tungsten lattice and in the unidentified X defects. Hence, D_1 is the line which passes through the annihilation characteristics in the lattice and in the monovacancy, and D_2 is characteristic of the presence of the V_p and X defects annihilation states.

D_1, but on the contrary they are all located on the D_2 straight line. This strongly suggests that only the X and the V_p positron traps are present in this sample annealed at 673 K, which signifies that almost all the primary radiation-induced defects V_1 disappeared (either by agglomeration or by annihilation at defects sinks). Hence, D_2 is characteristic of the presence of only the two positron annihilation states that are the V_p and X defects. Moreover, the fact that these positron annihilation characteristics move away from those in the X defects as positrons go deeper in the material indicates that the V_p defects concentration increases with depth. This is not surprising since the main vacancy source is located in the cascade region, which is in the present case deeper than the positron implantation depth. Summarizing, results obtained from the simulation allow pointing up that an annealing at low temperature leads to a drastic change in the radiation-induced vacancy like defects depth profile, which in turn should play a role on the helium retention.

Finally, as can be seen on Fig. 5 which shows the $S(W)$ plots corresponding to the mean S and W values obtained in the 23–25 keV positron energy range for the four fluences and the six temperatures, the behaviour observed for the 10^{16} cm^{-2} implanted tungsten sample can be directly transposed to the 5×10^{16} cm^{-2} fluence. Indeed, the corresponding $S(W)$ curves exhibit the same shape; in particular, in the two cases, all the $S(W)$ points tend to align, beyond 523 K, on the D_2 line, which means that the same vacancy like defects (V_p) are detected beyond the same temperature. Moreover, it clearly appears that the V_p concentration increases with the implantation fluence. This result can be easily explained considering that the probability to form large defects is directly linked to the probability for the monovacancies to meet, thus to the initial defects concentration. This also explains why the evolution is clearly marked for the two highest fluences contrary to the two lowest ones. Indeed, a small implantation-induced defects concentration implies a decrease in the potential V_p defects concentration, and the part of positron annihilations in the X defects can not then be neglected in the S and W values; moreover, the slope difference between D_1 and D_2 is quite weak. For these reasons, the S and W variations for the 10^{14} and 10^{15} cm^{-2} fluences appear very fine, and the presence of the two stages is not visible. However, it is worth noticing that at the highest annealing temperature (673 K), all the $S(W)$ plots, including the ones corresponding to the two lowest fluences, are aligned on the D_2 line (see Fig. 5), which indicates that the same new defects are detected in every cases, and tends to prove that the situation described for the highest fluences must be the same whatever the implantation fluence.

4. Conclusion

The behaviour of implantation-induced defects created in the track region of 800 keV ^{3}He ions in polycrystalline tungsten samples was studied by Doppler broadening spectroscopy as a function of annealing temperature. Four fluences were investigated, 10^{14}, 10^{15}, 10^{16} and 5×10^{16} cm^{-2}. The same evolution, but with a different magnitude, has been observed for the four fluences. The first annealing stage, which corresponds to the migration of monovacancies, was already observed in the past by several authors but at different temperatures ranging from 553 K to 873 K. In the present study, this stage is accurately found to occur between 523 K and 573 K; this result is a relevant data since it is a fundamental value in the framework of the wide study of the gases interaction with vacancy like defects in plasma-facing materials. Migration of these monovacancies leads to their disappearing, essentially by the formation of larger vacancy like defects, and the resulting defects depth profile is drastically altered. The helium retention properties of the material should be modified by these changes.

Acknowledgments

This study is financially supported by the department for the controlled fusion (DRFC) of CEA in the framework of the Sixth European **EURATOM** Framework Programme.

References

[1] H. Trinkaus, B.N. Singh, J. Nucl. Mater. 323 (2003) 229.
[2] P.M.G. Nambissan, P. Sen, Solid State Commun. 71 (1989) 1165.
[3] P.M.G. Nambissan, P. Sen, Rad. Eff. Defect Solid 124 (1991) 215.
[4] V.S. Subrahmanyam, P.M.G. Nambissan, P. Sen, Solid State Commun 89 (1994) 523.
[5] Shengyun Zhu, Yongjun Xu, Zhiqiang Wang, Yongnan Zheng, Dongmei Zhou, Enpeng Du, Daqing Yuan, M. Fukuda, M. Mihara, K. Matsuta, et al., J. Nucl. Mater. 343 (2005) 330.
[6] M.S. Abd el Keriem, D.P. van der Werf, F. Pleiter, Phys. Rev. B 47 (1993) 14771.
[7] A. van Veen, H. Eleveld, M. Partanen, F. Labohm, H. Schut, Mater. Sci. Forum 175–178 (1995) 229.
[8] R.W. Balluffi, J. Nucl. Mater. 69&70 (1978) 240.
[9] R.A. Johnson, Phys. Rev. B 27 (1983) 2014.
[10] P. Ehrart, in: H. Ullmaier (Ed.), Atomic Defects in Metals, Landolt–Bornstein New Series Group III/25, Springer-Verlag, Berlin, 1991.
[11] C.S. Becquart, C. Domain, Nucl. Instrum. and Meth. B 255 (2007) 23.
[12] N. Yoshida, H. Iwakiri, K. Tokunaga, T. Baba, J. Nucl. Mater. 337–339 (2005) 946.
[13] J.F. Ziegler, J.P. Biersack and U. Littmark in: The Stopping and Range of Ions in Solids, Pergamon, New York, 1985. <www.srim.org>.
[14] P. Desgardin, P. Desgardin, L. Liszkay, Marie-France Barthe, L. Henry, J. Briaud, M. Saillard, L. Lepolotec, C. Corbel, G. Blondiaux, A. Colder, P. Marie, M. Levalois, Mater. Sci. Forum 363–365 (2001) 523.
[15] P. Desgardin, M.-F. Barthe, E. Ntsoenzok, C.-L. Liu, Appl. Surf. Sci. 252 (2006) 3231.
[16] A. van Veen, H. Schut, J. de Vries, R.A. Hakvoort, M.R. Ijpma, in: P.J. Schultz, G.R. Massoumi, P.J. Simpson (Eds.), Positron Beams for Solids and Surfaces, AIP, New York, 1990.
[17] A. Debelle, M.-F. Barthe, T. Sauvage, R. Belamhawal, A. Chelgoum, P. Desgardin, H. Labrim, J. Nucl. Mater. 362 (2007) 181.
[18] A. Vehanen, P. Hautojärvi, J. Johansson, J. Yli-Kauppila, Phys. Rev. B25 (1982) 762.